

Local Dynamics and Strong Correlation Physics I: 1D and 2D Half-filled Hubbard Models

Tudor D. Stanescu and Philip Phillips
Loomis Laboratory of Physics
University of Illinois at Urbana-Champaign
1100 W.Green St., Urbana, IL, 61801-3080

We report on a non-perturbative approach to the 1D and 2D Hubbard models that is capable of recovering both strong ($U \gg t$) and weak-coupling ($U \ll t$) limits, with U the on-site Coulomb repulsion and t the kinetic energy. Dynamical corrections to the electron self-energy in the single particle Green function are explicitly included by expanding in terms of the 16 eigenstates that characterise two nearest neighbour sites. We first show that even when U is much smaller than the bandwidth, the Mott-Hubbard gap never closes at half-filling in both 1D and 2D. Consequently, the Hubbard model at half-filling is always in the strong-coupling non-perturbative regime. For both large and small U , we find that the population of nearest-neighbour singlet states approaches a value of order unity as $T \rightarrow 0$ as would be expected for antiferromagnetic order. We also find that the double occupancy is a smooth monotonic function of U and approaches the anticipated non-interacting limit of $1/4$ as $U \rightarrow 0$ and vanishes as $U \rightarrow \infty$. Finally, we compute the heat capacity ($C(T, U)$) for both 1D and 2D. Our results for 1D at moderate to high temperatures are in quantitative agreement with those of the exact Bethe ansatz solution, differing by no more than 1%. In addition, we find that in 2D, the $C(T, U)$ curves vs T for different values of U exhibit a universal crossing point at two characteristic temperatures, $T \approx 1.7t \pm 0.1t$ and $T \approx 0.4 \pm 0.1t$ as is seen universally in Hubbard models and experimentally in a wide range of strongly-correlated systems such as ${}^3\text{He}$, $U\text{Be}_3$, and $\text{CeCu}_{6-x}\text{Al}_x$. The success of this method in recovering well-established results that stem fundamentally from the Coulomb interaction suggests that local dynamics are at the heart of the physics of strongly correlated systems.

I. INTRODUCTION

In both the weak and strong coupling regimes, the Hubbard model at half-filling is expected to be an antiferromagnet at $T = 0$. The strong-coupling argument relies on an isomorphism between the half-filled Hubbard model in the limit that the on-site Coulomb repulsion, U , exceeds the hopping integral, t , and a Heisenberg antiferromagnet. As a consequence, the corresponding ground state is antiferromagnetic and the energy scale for the gap between the upper and lower Hubbard bands is set by the energy cost for double occupancy, $\Delta \approx U$. In the opposite or weak-coupling limit, $U \ll t$, perturbation theory predicts that a van-Hove singularity induces a spin-density wave producing a gap that is exponentially small in the Coulomb repulsion; that is, $\Delta \approx t e^{-2\pi\sqrt{t/U}}$. While the perturbative argument cannot be extended into the strong-coupling regime where the t/U mapping to a perfect Heisenberg antiferromagnet applies, continuity between the two regimes suggests that antiferromagnetism persists for any non-zero value of U . Further, this argument would also suggest that the Hubbard gap never closes for any non-zero value of U . Consequently, the half-filled Hubbard model is always in the strong-coupling regime. However, no exact results are known. In fact, while numerical simulations [1] support an antiferromagnet at half-filling, several mean-field arguments suggest otherwise. Dating back to the pioneering work of

Mott [2] and Brinkman and Rice [3], numerous calculations on the 2D [4,5] or the $D = \infty$ [6,7] half-filled Hubbard models suggest that whenever U is much smaller than the bandwidth, $W = 8t$, the Hubbard gap closes and a metallic phase ensues. Contrastly, Anderson [8] has argued that almost certainly the half-filled 2D Hubbard model is non-perturbative as in the 1D case [9], thereby possessing a discontinuity only at $U = 0$. At the heart of the non-perturbative nature of the Hubbard model [8] is the projective mismatch between the low-energy physical subspace and the “anti-bound states” which form in 2D for any non-zero value of U . Antiferromagnetism follows necessarily as a corollary from the break-down of perturbation theory.

In this paper we re-examine this problem using an approach that is capable of spanning the weak and strong-coupling regimes. Our approach is based on the Hubbard operators which exactly diagonalize the interaction part of the Hubbard Hamiltonian. Consequently, the Hubbard operators are tailor-made to access the strong-coupling regime, $U \gg t$. Rather than work in the static approximation in which quantum fluctuations are ignored leading to infinitely sharp upper and lower Hubbard bands, we include the dynamical corrections which lead to broadening of the spectral features. As in the work of Matsumoto and Mancini [10,11], we focus on the dynamics associated with two neighbouring sites. The dominant dynamics appear to be governed by spin-fluctuations which lead to singlet-triplet excita-

tions. From our analysis, we conclude that the Hubbard gap never closes and the 2D Hubbard model at half-filling is always in the strong-coupling regime. Our results then corroborate those of a recent improvement [12] on dynamical mean-field theory [7] in which the momentum-dependence of the self-energy is explicitly included [12] at particular points in the Brillouin zone. To determine the validity of the approach we use here, we study as well the 1D half-filled Hubbard model as exact results are known from Bethe ansatz [13]. As expected, we find that the Hubbard gap persists even in the weak coupling regime. In addition, we find that our results for the heat capacity are in perfect agreement with those from Bethe ansatz in the temperature range where the Coulomb interaction dominates the physics, that is, moderate to high temperatures. Finally, we show that we recover the well-established universal crossing [14–16] of $C(T, U)$ vs T for various values of U that is seen experimentally in a wide range of strongly-correlated systems such as ${}^3\text{He}$ [17], $\text{CeCu}_{6-x}\text{Al}_x$ [18], $\text{Nd}_{2-x}\text{Ce}_x\text{CuO}_4$ [19], and UBe_3 [20]. The success of our approach suggests that local dynamics lead to many of the features of strongly-correlated electronic systems.

II. DYNAMICAL GREEN FUNCTION APPROACH

The starting point of our analysis is the on-site Hubbard model

$$H = - \sum_{i,j,\sigma} t_{ij} c_{i\sigma}^\dagger c_{j\sigma} + U \sum_i n_{i\uparrow} n_{i\downarrow} \quad (1)$$

where $t_{ij} = t$ if (i, j) are nearest-neighbour sites and zero otherwise. Rather than working with the original electron operators, we use the Hubbard operators $\eta_{i\sigma} = c_{i\sigma} n_{i-\sigma}$ and $\xi_{i\sigma} = c_{i\sigma} (1 - n_{i-\sigma})$ as these operators exactly diagonalise the interaction term. In terms of the Hubbard operators, $c_{i\sigma} = \eta_{i\sigma} + \xi_{i\sigma}$. While the interaction term is now simplified in this basis, the Hubbard operators do not obey standard Fermi statistics, making impossible any diagrammatic approach based on Wick's theorem. However, the equation of motion approach has been demonstrated [21–23] to offer an alternative to the diagrammatic expansion. Consider the two-component basis

$$\psi_\sigma(i) = \begin{pmatrix} \xi_{i\sigma} \\ \eta_{i\sigma} \end{pmatrix} \quad (2)$$

and its associated Green function $G(i, j, t, t') = \langle\langle \psi_{i\sigma}; \psi_{j\sigma}^\dagger \rangle\rangle = \theta(t - t') \langle\{ \psi_{i\sigma}(t), \psi_{j\sigma}^\dagger(t') \}\rangle$ where $\{A, B\}$ is the anticommutator and $\langle \dots \rangle$ is the thermal average. The equations of motion for the Hubbard operators,

$$j_i(t) = i \frac{\partial \psi_i}{\partial t} = E_0 \psi_i + \delta j_i^0 \quad (3)$$

will of course contain a contribution which is linear in the Hubbard basis and in addition new terms, δj_i^0 which contain operators that lie outside the Hubbard basis. Ideally, if such operators are included in the Hubbard basis, then the non-linear contributions can be minimized. However, such a procedure is necessarily cumbersome. Instead of enlarging the basis, we project δj_i^0 onto the Hubbard basis using the Roth [22] projector,

$$\mathcal{P}(O) = \sum_{ln} \langle\{O, \psi_l^\dagger\}\rangle I_{ln}^{-1} \psi_n \quad (4)$$

which projects any operator O onto the Hubbard operator basis, where $I(\mathbf{k}) = FT \langle\{ \psi_\sigma(i, t), \psi_\sigma^\dagger(j, t) \}\rangle$, and FT denotes the time and space Fourier transform. This projector is particularly useful because it allows us to recast the equations of motion for the Hubbard operators

$$j_i(t) = E_0 \psi_i + \mathcal{P}(\delta j_i^0) + \delta j_i = E \psi_i + \delta j_i \quad (5)$$

in terms of the renormalized energy matrix

$$E(\mathbf{k}) = E_0 + FT \langle\{ \delta j_{i\sigma}^0, \psi_{l\sigma}^\dagger \}\rangle I^{-1}(\mathbf{k}) \quad (6)$$

and a correction $\delta j_i = \delta j_i^0 - \mathcal{P}(\delta j_i^0)$. Clearly, $\mathcal{P}(\delta j_i) = 0$. The formal solution for the Fourier transform of the Green function

$$G(\mathbf{k}, \omega) = \frac{1}{\omega - E(\mathbf{k}) - \delta m(\mathbf{k}, \omega)} I(\mathbf{k}) \quad (7)$$

contains the dynamical self-energy,

$$\delta m(\mathbf{k}, \omega) = FT \langle R \{ \delta j_{i\sigma}(t), \delta j_{l\sigma}^\dagger(t') \} \rangle I \quad (8)$$

where R denotes retarded and I the irreducible part. For a paramagnetic phase, the overlap matrix

$$I = \begin{pmatrix} 1 - \frac{n}{2} & 0 \\ 0 & \frac{n}{2} \end{pmatrix} = \begin{pmatrix} I_1 & 0 \\ 0 & I_2 \end{pmatrix} \quad (9)$$

is explicitly diagonal. The weights which appear along the diagonal represent the contribution from the lower and upper Hubbard bands, respectively. Note, they sum to unity. This feature coupled with the fact that the dynamical corrections vanish when $U = 0$ guarantees that we recover the correct non-interacting limit.

The primary operational hurdle with any analytical approach to the Hubbard model is the evaluation of the dynamical self energy. In the static approximation [21–23], the self-energy is dropped, and the Green function reduces to the pole structure

$$G(\mathbf{k}, \omega) = \frac{1}{\omega - E(\mathbf{k})} I(\mathbf{k}) \quad (10)$$

where $E(\mathbf{k})$ defines the energy bands. At this level of theory, the Hubbard bands are sharp as the Green function has a pole at the energy of each band. As our focus, however, is on the closing of the Hubbard gap, the pole

approximation is inadequate and the broadening in the bands arising from the self energy is crucial. In the context of the composite operator approach, Mancini and Matsumoto [10] have developed a real-space scheme for computing the dynamical corrections to the static approximation. To implement this procedure, we rewrite the dynamical correction

$$\begin{aligned} \delta m(\mathbf{k}, \omega) &= Dm(\mathbf{k}, \omega) \begin{pmatrix} 1 & -1 \\ -1 & 1 \end{pmatrix} \\ &\equiv FT \langle R \delta j_i(t) \delta j_l^\dagger(t) \rangle \hat{\mathbf{K}} \end{aligned} \quad (11)$$

in terms of the 2×2 matrix K . Because $Dm(\mathbf{k}, \omega)$ cannot be evaluated exactly, we seek a systematic way of calculating the dynamical corrections. The simplest approach would be to consider the single-site approximation. Such an approximation is in the spirit to the $d = \infty$ [6] methods in which the self-energy is momentum independent. An improvement would be to consider the dynamics associated with two sites as proposed by Mancini and Matsumoto [10,11]. Evaluation of the self-energy over successively larger clusters would lead to an exact determination of the dynamical corrections. Hence, we write the dynamical corrections as a series

$$Dm(x, x') = \delta_{x,x'} Dm_0(x, x') + \sum_a \delta_{x+a,x'} Dm_1(x, x') + \dots$$

in increasing cluster size. Here, x and x' are neighbouring sites and a indexes all nearest-neighbour sites. In the two-site approximation, the series is truncated at the level of on-site, Dm_0 , and nearest-neighbour, Dm_1 contributions. In Fourier space, the dynamical corrections can be written as,

$$Dm(\mathbf{k}, \omega) \approx Dm_0(\omega) + \alpha(\mathbf{k}) Dm_1(\omega) \quad (12)$$

with

$$\begin{aligned} Dm_0(\omega) &= \frac{1}{4} FT \langle R \{ \delta j(t), \delta j^\dagger(t') \} \rangle, \\ Dm_1(\omega) &= \frac{1}{4} FT \langle R \{ \delta j(t), \delta j'^\dagger(t') \} \rangle, \end{aligned} \quad (13)$$

where the factor of $1/4$ arises from the coordination number on a square lattice, $\alpha(\mathbf{k}) = (\cos k_x + \cos k_y)/2$, and δj and $\delta j'$ are centered on x and x' , respectively. The goal here is to study the half-filled Hubbard model by evaluating Dm_0 and Dm_1 in the two-site approximation.

Because the procedure for implementing the two-site approximation has been described previously [10,11], we will only outline the essence of the method: 1) enumerate the quantum mechanical states for two neighbouring sites, 2) use the resolvent method [24] to express how the surrounding environment interacts with the two-site system, 3) express the δj 's in terms of the level operators for the two-site system, and 4) use the non-crossing approximation to expand $Dm(\mathbf{k}, \omega)$ in terms of the two-site

states. For two sites, there are $4^2 = 16$ electronic states. Let $B(i)$, $F_\sigma(i)$, and $D(i)$, represent single site level operators acting on empty (a boson state), singly (with spin σ) and doubly occupied sites respectively. In terms of the level operators, the original Hubbard operators are $\xi_\sigma = B^\dagger F_\sigma$ and $\eta_\sigma = \sigma F_{-\sigma}^\dagger D$. The level operators for two-site states, Φ_n , are formed by all possible symmetric and antisymmetric combinations of B , F_σ and D on two neighbouring sites. Two particular states of interest are the singlet

$$FF_A = \frac{F_\uparrow F'_\downarrow - F_\downarrow F'_\uparrow}{\sqrt{2}} \quad (14)$$

and triplet state formed from three states,

$$FF_S = \frac{F_\uparrow F'_\downarrow + F_\downarrow F'_\uparrow}{\sqrt{2}}, \quad (15)$$

as well as $F_\uparrow F'_\uparrow$ and $F_\downarrow F'_\downarrow$. The two-site system described by all sixteen states of this form is not isolated. The rest of the system acts as a reservoir. The coupling is realized through the electron propagator for the rest of the system, which can be obtained from the appropriate trace of the single-particle Green function defined in Eq. (7). Consequently, the energy levels of the two-site states are broadened. We define then the resolvent of a two-site state, $R_{nm}(t) = \theta(t) \langle \langle \Phi_n(t) \Phi_m^\dagger(0) \rangle \rangle$, as a trace over the degrees of freedom of the reservoir and the two-site subsystem. The Fourier transform of the resolvent

$$R_{nm} = \int d\omega' \frac{\sigma_{nm}(\omega')}{\omega - \omega' + i\delta}. \quad (16)$$

can be written in terms of the spectral function for the two-site system, which is defined as $\sigma_{nm} = -\text{Im}R_{nm}/\pi$. The δj 's are then expanded

$$\delta j = \sum_{nm} a_{nm} \Phi_n^\dagger \Phi_m \quad (17)$$

in terms of the sixteen level operators that describe the two-site physics. The products of δj 's that comprise the dynamical corrections are then expressed in terms of the two-site resolvents using the non-crossing approximation (NCA). Consequently, the total self-energy contains all the possible convolutions of the two-site resolvents. As the dynamics included are local, the NCA is expected to be accurate [24]. The resolvents associated with local triplet and singlet states are sharply peaked at well-defined energies [10]. The energy difference is small, however, and given roughly by t^2/U . Consequently, singlet-triplet mixing cannot be ignored. We can introduce this spin-fluctuation effect as a correction to the self-energies of the resolvents. The effective energy of the exchange interaction is given by the difference,

$$J \equiv \int_{-\infty}^{\infty} \omega (\sigma_{FF_S} - \sigma_{FF_A}) d\omega, \quad (18)$$

of the first moments of the spectral functions for the singlet and triplet two-site states. Antiferromagnetism corresponds to $J > 0$. To facilitate a self-consistent evaluation of the exchange energy, we computed the equations of motion for the two-site level operators in the presence of the spin-fluctuation term, $J\mathbf{n} \cdot \mathbf{n}^\alpha/2$. Here $\mathbf{n} = (c_{i\uparrow}, c_{i\downarrow})\sigma_i(c_{i\uparrow}, c_{i\downarrow})^\dagger$, with σ_i the Pauli matrices and α represents an average over the nearest neighbours of the second site in the cluster exclusive of the first site. A final quantity that is needed is the occupancy in the two-site states

$$n_{\Phi_n} = Z_{\Phi_n}/Z, \quad (19)$$

where $Z_{\Phi_n} = \int d\omega \bar{\sigma}_{nm}(\omega)$, where Z represents a sum over all Z_{nm} 's for the sixteen states and $\bar{\sigma}_{nm} = \exp(-\beta\omega)\sigma_{nm}(\omega)$.

III. RESULTS

To obtain a self-consistent solution for the self-energy, we start with an initial guess for the electron spectral function which will be used to describe the properties of the environment in which the two-site system is placed. The two-site resolvents are then determined iteratively. Once the resolvents are determined, they are fed into the dynamical corrections and the Green function is determined. A new spectral function is then computed thereby closing the self-consistent set of equations. This procedure is repeated until convergence is reached.

A. Hubbard gap

Shown in Fig. (1) is the total electron spectral function $(-\text{Im}(G_{11}(k, \omega) + 2G_{12}(k, \omega) + G_{22}(k, \omega))/\pi)$ for the half-filled Hubbard model for $U = 8t$ and $T = 0.15t$. Each trace corresponds to a momentum starting from $(0, 0)$ to (π, π) to $(\pi, 0)$ and then back to $(0, 0)$. Clearly shown are the upper and lower Hubbard bands with an energy gap of order U and the flatness of the band near the $(\pi, 0)$ point. The broadening is due entirely to the dynamical corrections. In the absence of such processes, the spectral function would correspond to a series of δ -functions at the lower and upper Hubbard bands. In the upper Hubbard band, the dominant spectral weight lies at the (π, π) point whereas in the lower band the spectral weight is located at $(0, 0)$. Broad spectral features obtain near the $(\pi, 0)$ point. The analogous spectral function for the $D=1$ case is shown in Fig. (2). As in the 2D case, the energy separation between the lower and upper Hubbard bands for $D=1$ is striking. In both cases, the periodicity of the band is 2π as is expected for a paramagnetic solution. Nonetheless, we will show that local antiferromagnetic correlations exist.

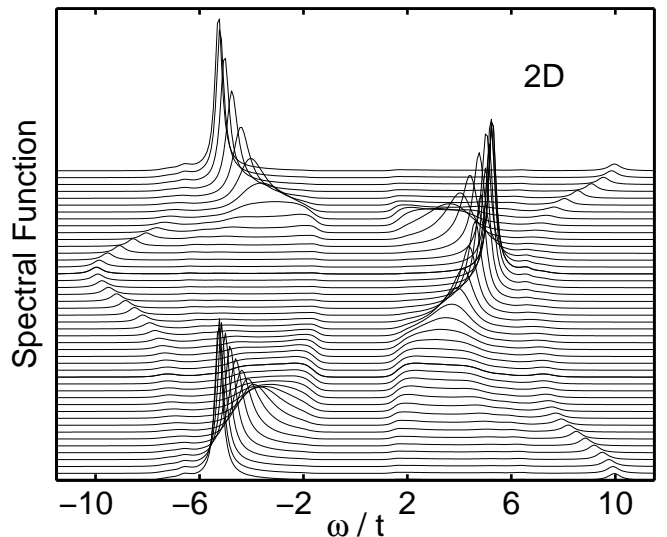


FIG. 1. Momentum and energy dependence of the electron spectral function for $U = 8t$ and $T = 0.15t$ for different values of \mathbf{k} . From top to bottom, the momenta correspond to $(k_x, k_y) = (0, 0) \rightarrow (\pi, \pi) \rightarrow (\pi, 0) \rightarrow (0, 0)$. Each momentum trace is shifted by hand.

Integration of the spectral functions with respect to momentum yields the density of states (DOS) as a function of energy shown in Figs. (3) and (4).

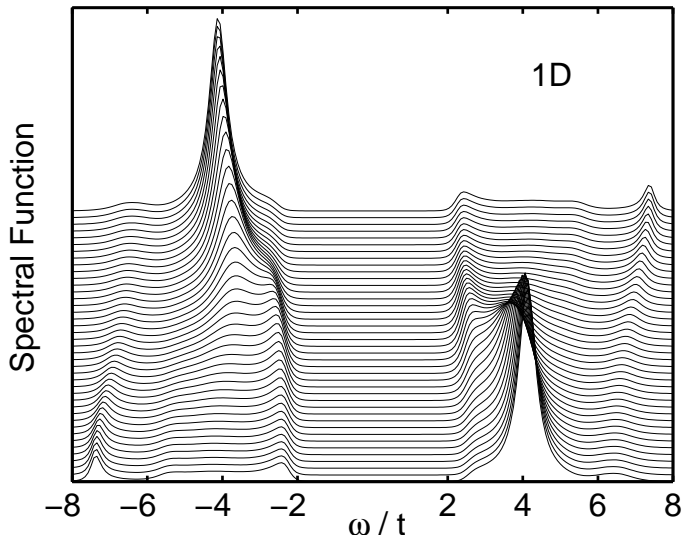


FIG. 2. Momentum and energy dependence of the electron spectral function for $U = 8t$ and $T = 0.15t$ for different values of \mathbf{k} . From top to bottom, the momenta correspond to $k_x = 0 \rightarrow \pi$. Each momentum trace is shifted by hand.

It is evident that the Hubbard gap is fully formed for $U \approx W$, where W is the bandwidth ($W = 4t$ for $D = 1$ and $W = 8t$ for $D = 2$). In the $D=1$ case, the gap is wider than in $D = 2$. For all values of U , we see a clear suppression in the density of states near zero energy. However, for small values of U , the density of states at the Fermi

energy does not vanish at the temperatures we consider here. It is crucial then that we investigate the temperature dependence of the density of states at zero energy for small U . Shown in Fig. (5) is the density of states at the Fermi energy, $\rho(0)$ as a function of temperature for both 1D and 2D at $U = 2t$.

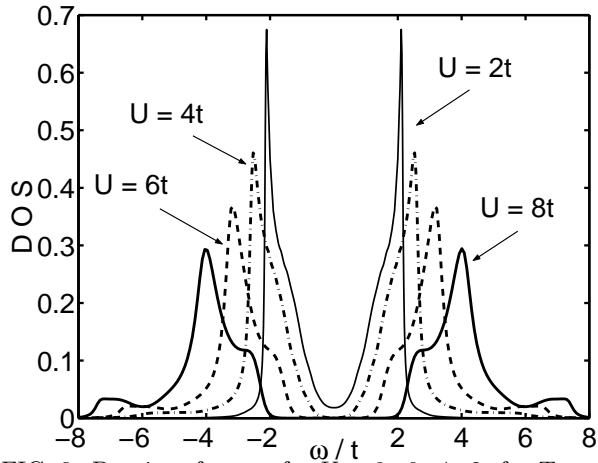


FIG. 3. Density of states for $U = 8t, 6t, 4t, 2t$ for $T = .15t$ in $D=1$. The presence of a gap for all values of U indicates an absence of a metallic state at half-filling.

For both $D = 1$ and $D = 2$, $\rho(0)$ drops to zero as the temperature decreases. The enhancement seen in the density of states at zero energy in the $D = 2$ case over the $D = 1$ problem is tied to the shape of the non-interacting density of states. In $D=1$, as U decreases, the density of states becomes sharp (and actually diverges) at the band edges rather than approaching a constant value as for $D = 2$. In fact, in $D = 2$, the band exhibits a singularity at the gap edge. Consequently, it is easier to fill in the gap in $D=2$ than in $D=1$ as is seen in Fig. (5). This trend also persists for any value of U as demonstrated in Fig. (6) for $U = 8t$.

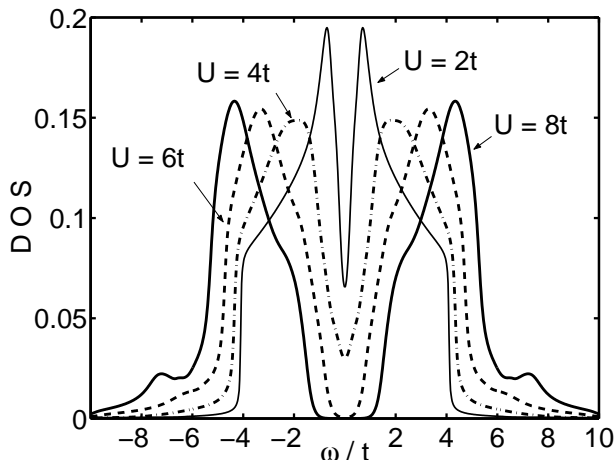


FIG. 4. Density of states for $U = 8t, 6t, 4t, 2t$ for $T = .15t$ in $D = 2$. The presence of a gap for all values of U indicates an absence of a metallic state at half-filling.

We see clearly that $\rho(0)$ is non-zero even in the strong-coupling regime, $U \gg t$, provided that the temperature is sufficiently large. This signifies that the physics at small and large U do not differ qualitatively. Because we have probed both $U < W$ and $U > W$, we conclude that the Hubbard gap persists for all values of U both in $D = 1$ and $D = 2$ and is certainly fully formed at $T = 0$. Hence, the only singular point in the half-filled Hubbard model is $U = 0$ where the gap disappears. Consequently, there is an absence of a metallic state at half-filling. This result is in agreement with that of Moukouri and Jarell [12] and is consistent with the argument of Anderson [8] that the Hubbard model is always in the strong-coupling regime.

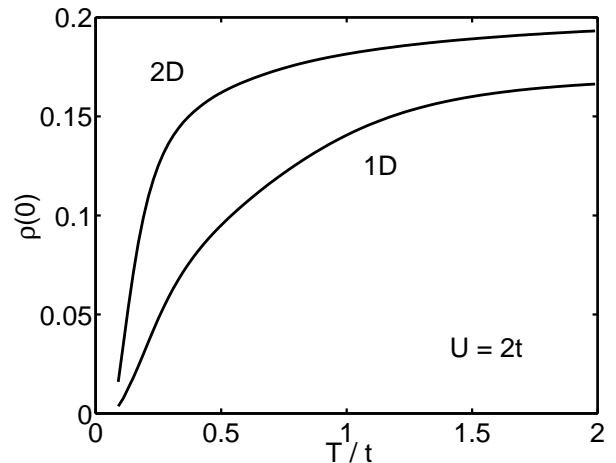


FIG. 5. Density of states at the Fermi energy for $U = 2t$ as a function of temperature.

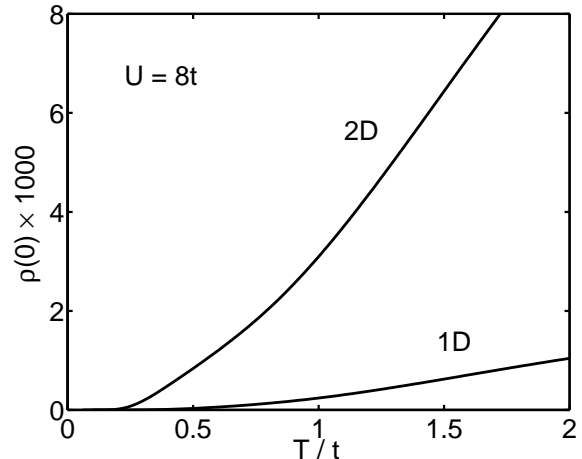


FIG. 6. Density of states at the Fermi energy for $U = 8t$ as a function of temperature.

Additional confirmation of the continuity between the weak and strong coupling regimes at half-filling is seen from the double occupancy shown in Fig. (7). In terms of the two-site resolvents, the expression for the double occupancy is given by

$$D = \frac{1}{2}(n_{FDS} + n_{FDA} + n_{DBS} + n_{DBA}) + n_{DD} \quad (20)$$

where n_ϕ is given by Eq. (19). In both cases, the double occupancy smoothly approaches the non-interacting value of $1/4$ as U decreases. The absence of any kink in the double occupancy indicates an absence of a phase transition between the regimes, $U < W$ and $U > W$. Hence, a continuity appears to exist between the small and large U regimes in the half-filled Hubbard models. The existence of a non-perturbative gap indicates that half-filled 1D and 2D Hubbard models flow to strong coupling.

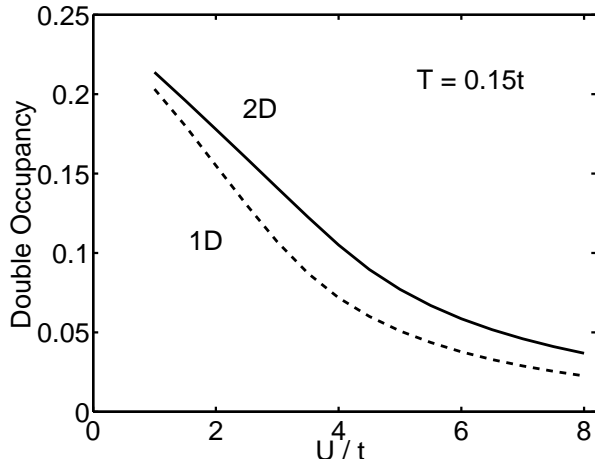


FIG. 7. Double occupancy as a function of U . In both $D=1$ and $D=2$, the double occupancy approaches the non-interacting value of $1/4$ as $U \rightarrow 0$ and vanishes as $U \rightarrow \infty$.

B. Local Antiferromagnetism

Because our method is capable of unclocking the underlying spin dynamics, we investigated the behaviour of the local triplet, n_{FFS} , and singlet, n_{FFA} , occupancies for the states defined in Eqs. (15) and (14), respectively. These quantities were computed directly from the resolvents that enter Eq. (19). Should the ground state be an antiferromagnet, the singlet occupancy, n_{FFA} , should exceed the triplet occupancy, n_{FFS} at sufficiently low temperatures. For both 1D and 2D the plots of the singlet and triplet occupancies are shown in Figs. (8) and (9), respectively.

As is evident, $n_{FFA} > n_{FFS}$ as is consistent with an ordering tendency toward antiferromagnetism. Notice in the large U limit in 2D, singlet state formation is enhanced over the 1D value. However, to ascertain if these local probes are true signatures of ground state properties, we computed the temperature dependence of n_{FFS} and n_{FFA} for both 1D and 2D at $U = 8t$.

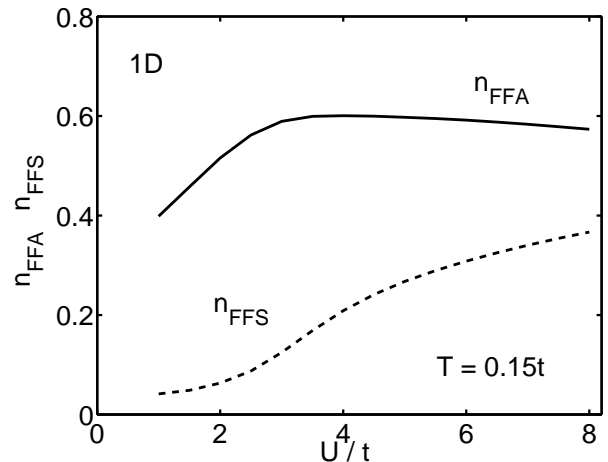


FIG. 8. Singlet (n_{FFA}) and triplet (n_{FFS}) state occupancies as a function of U/t for $D=1$. For any non-zero value of U , $n_{FFA} > n_{FFS}$ indicating a tendency toward antiferromagnetic order.

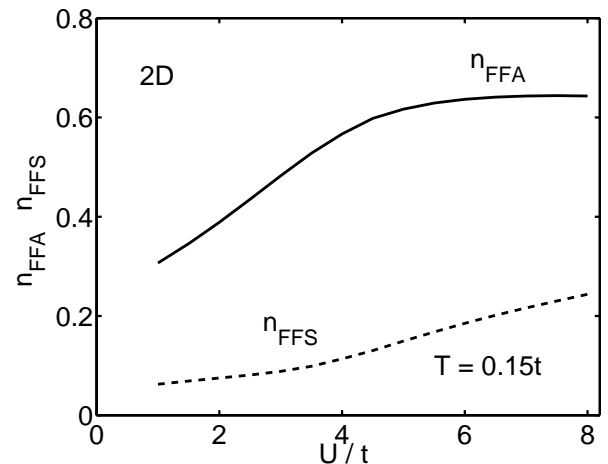


FIG. 9. Singlet (n_{FFA}) and triplet (n_{FFS}) state occupancies as a function of U/t for $D=2$. For any non-zero value of U , $n_{FFA} > n_{FFS}$ indicating a tendency toward antiferromagnetic order.

From Figs. (10) and (11), we find that at high temperatures triplet excitations dominate. However, this trend is reversed below some temperature and the singlet occupancy becomes of order unity. This is significant and implies that the ground state is in fact an antiferromagnet. The tendency toward antiferromagnetism appears to be slightly enhanced in 2D relative to the 1D problem. Our results then are consistent with antiferromagnetic order at $T = 0$ in both 1D and 2D.

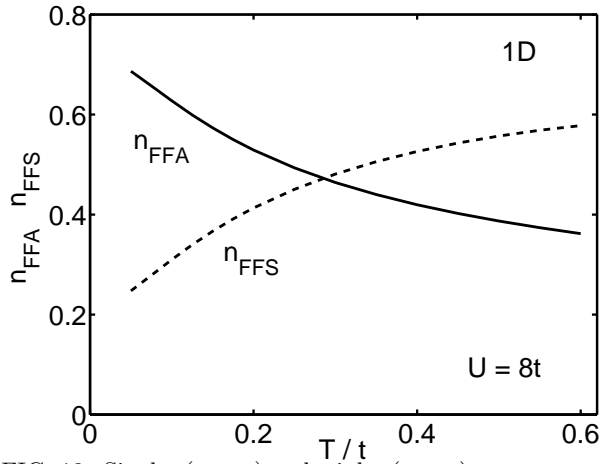


FIG. 10. Singlet (n_{FFA}) and triplet (n_{FFS}) state occupancies as a function of temperature for $D=1$. The fact that the singlet occupancy as $T \rightarrow 0$ becomes of order unity is consistent with antiferromagnetic order.

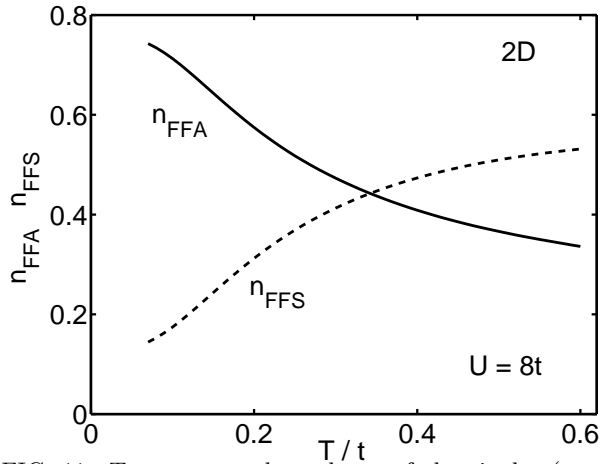


FIG. 11. Temperature dependence of the singlet (n_{FFA}) and triplet (n_{FFS}) occupancies for $D=2$. The fact that the singlet occupancy as $T \rightarrow 0$ becomes of order unity is consistent with antiferromagnetic order.

The energy splitting between the singlet and triplet states is due to an effective exchange interaction. Using Eq. (18), we computed the effective exchange interaction shown in Fig. (12) for both 1D and 2D. Note first that J is always positive as a consequence of the fact that the singlet state is lower in energy than the triplet. This is a further indication of the antiferromagnetic order in the ground state. As expected, J is well approximated by t^2/U in the strong-coupling regime. However, as U decreases, deviations from this behaviour are observed.

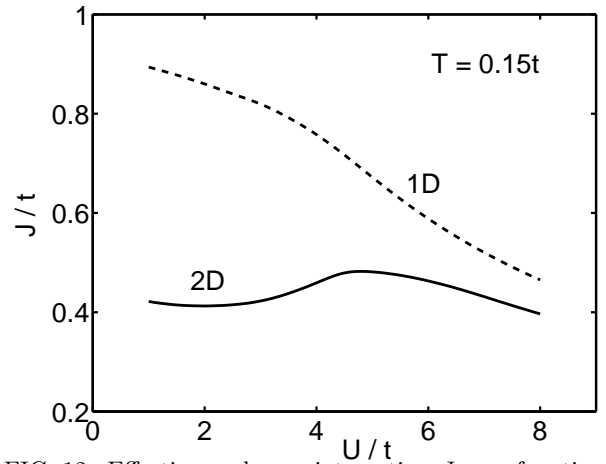


FIG. 12. Effective exchange interaction J as a function of U/t computed using Eq. (18).

C. Heat Capacity

The natural question that arises with any approximate treatment of strong correlation physics is: How seriously should the results be taken? Our study of the 1D problem is in part motivated by the fact that exact results are available from the Bethe ansatz. While Bethe ansatz is not amenable to yielding the Green functions from which the density of states can be calculated, ground state energies and thermodynamic quantities are readily available by this technique. Rather than compare with the total energy, we compute the temperature derivative or the heat capacity. Computation of the average energy is straightforward because we have already obtained the average double occupancy. Shown in Fig. (13) is a comparison between the heat capacity computed within the present method (solid line) and the prediction from the Bethe ansatz [13] (triangles) for $U = 8t$.

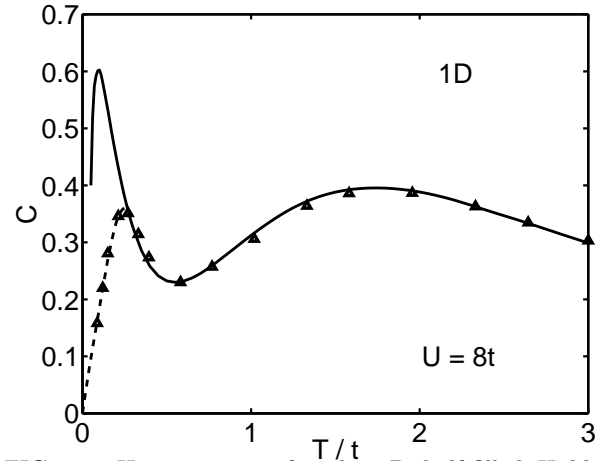


FIG. 13. Heat capacity for the 1D half-filled Hubbard model as a function of temperature for $U = 8t$. The filled triangles are the results from the exact treatment via Bethe ansatz (see Ref. ([13])).

This figure demonstrates that at high to moderately low temperatures, the present method is quantitatively accurate, yielding results which differ by no more than 1% from those of the Bethe ansatz. Such agreement is significant because in 1D, correlation effects are particularly amplified. The two-peak structure of the heat capacity is tied to a competition between the contribution from the potential energy (high T) and the kinetic energy (low T) as illustrated in Fig. (14).

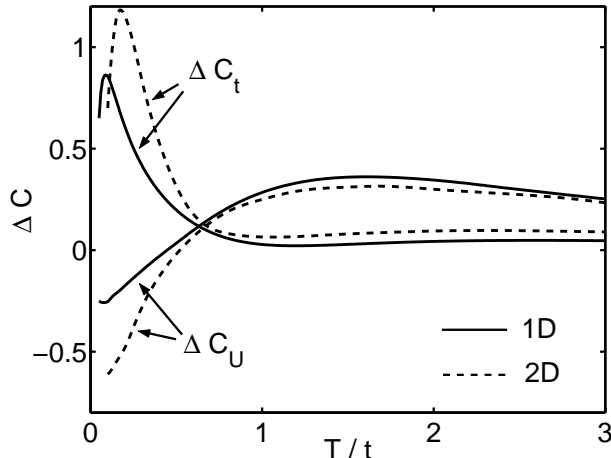


FIG. 14. Kinetic (ΔC_t) and potential (ΔC_U) energy contributions to the heat capacity of the 1D and 2D half-filled Hubbard models for $U = 8t$.

Both display maxima but in distinctly different energy regimes. Near perfect agreement with the Bethe ansatz solution is obtained at high temperatures where the potential energy dominates. This is to be expected as the Hubbard operators provide an accurate treatment of the potential energy but only an approximate description of the kinetic energy. At sufficiently low temperatures, where the kinetic energy dominates, sharp spectral features appear and the numerical accuracy of the method wanes. Another source of error could be the two-site approximation itself. At low temperatures, an accurate description of the low-energy physics becomes essential. It might be that the two-site approximation inherently over-estimates the magnitude of the kinetic energy. To see if this breakdown persists for small U , we computed the heat capacity for $U = 2t$. The two-peak structure that occurs in the large U regime is absent for $U \ll W$ as illustrated in Fig. (15). The disappearance of the two peaks is dictated by the non-interacting limit which possesses a single peak at $T \approx 0.5t$. Our results are in quantitative agreement with the numerical simulations of Shiba and Pincus [26] down to $T \approx .1t$. Below this temperature, lack of numerical precision prohibited any accurate determination of the heat capacity. It appears then that the source of the breakdown at low temperatures stems more from the lack of numerical accuracy than from the local description of the physics. However,

more studies on this are necessary.

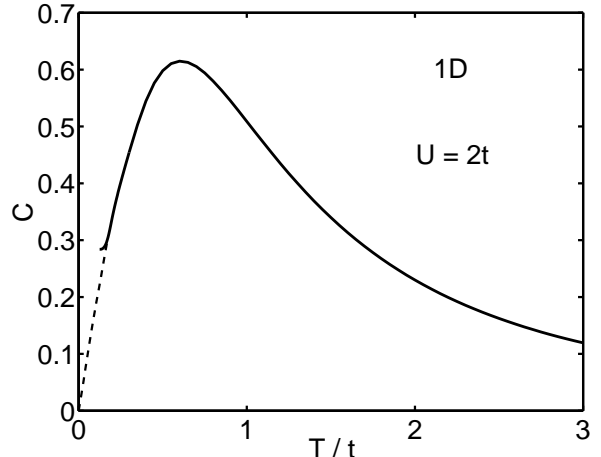


FIG. 15. Heat capacity for the 1D half-filled Hubbard model as a function of temperature for $U = 2t$. The deviation from the dashed line at low temperature stems from the emergence of sharp spectral features below $T \approx 0.1t$ which prohibit an accurate numerical determination of the integral that enter the heat capacity.

In 2D, the heat capacity (see Fig. (16)) has the familiar 2-peak structure of the 1D problem. Here again, this structure arises from a competition between the kinetic and potential energies as the dashed lines in Fig. (14) reveal. Similar results have also been obtained by Scalettar and colleagues [27] from quantum Monte Carlo simulations on finite samples. The final feature on which we focus is the crossing of $C(T, U)$ versus T for various values of U . In 1D comparison of Fig. (13) with (15) reveals that the heat capacities cross both at high temperature and at low temperature. Fig. (16) reveals that that this trend persists in 2D as well. The high temperature crossing point occurs at roughly $T \approx 1.7t \pm 0.1t$ whereas the low-temperature crossing point is $T \approx .4t \pm 0.1$. The errors are due largely to the uncertainty in the data at small U . In the quantum Monte Carlo studies of Duffy and Moreo [15] on a 6×6 square lattice, similar values for the low and high temperature crossing points were found as well. In the $D \rightarrow \infty$ limit [14,16], two crossing points are observed as well though at substantially smaller temperatures than in the 2D case. A unique crossing point for $C(T, U)$ as a function of T for different values of U implies that at a particular temperature, the heat capacity is independent of U . This behaviour is observed in a wide variety of strongly-correlated experimental systems, such as ${}^3\text{He}$ [17], $\text{CeCu}_{6-x}\text{Al}_x$ [18], $\text{Nd}_{2-x}\text{Ce}_x\text{CuO}_4$ [19], and UBe_3 [20]. Vollhardt [16] has shown that independence of $C(T, U)$ on U at a particular temperature is fundamentally rooted in strong correlation physics. The condition for a unique crossing point for $C(T, U)$ versus T for various values of U can be recast [16] as

$$0 = \int_0^\infty \frac{dT}{T} \frac{\partial C(T,U)}{\partial U} \quad (21)$$

in the limit that $T \rightarrow \infty$. At high temperatures, $C(T,U) \propto U/T$. Hence, $\partial C/\partial U > 0$ as $T \rightarrow \infty$. However, for the sum rule given by Eq. (21) to hold, $\partial C/\partial U$ must change sign as the temperature is lowered. Such sign changes will be mediated by terms proportional to higher powers of U that enter with opposing signs. Hence, the sign change of $\partial C/\partial U$ is a true correlation effect arising from terms at least proportional to U^2 and higher in the internal energy, $E(T,U)$. As there is no phase transition as a function of temperature, the curves for $C(T,U)$ must cross to satisfy the vanishing of the integral in Eq. (21). At low T , the width of the crossing point is determined by low-lying excitations generated by the kinetic energy. The natural scale for such excitations is $4t^2/U$, in rough agreement with the low temperature crossing point in Fig. (16). At high T , charge excitations dominate the contribution to the heat capacity. At large U , the gap should scale as $U - W$.

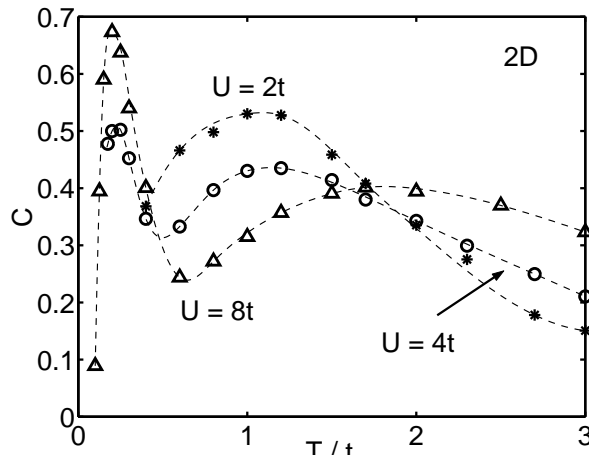


FIG. 16. Heat capacity for the 2D half-filled Hubbard model as a function of temperature for $U = 2t, 4t, 8t$. The crossing points at $T \approx 1.7t \pm 0.1t$ and at $T = .4t \pm 0.1t$ is in agreement with the general arguments of Ref. ([16]). The low-T peak in the heat capacity arises from spin fluctuations and the high temperature physics is tied to charge fluctuations.

IV. CLOSING REMARKS

We have applied a local method [10,11] to the determination of the dynamical corrections to the self-energy in the single-particle Green function for the 1D and 2D Hubbard models. Although this method focuses on local 2-site correlations, it captures such established features as the onset of antiferromagnetism, absence of a Mott-Hubbard transition for non-zero U , and the universal crossing of the heat capacity as a function of T for various values of U . As these features are the signatures

of strong-correlation at half-filling, it appears that local dynamics offer an adequate description of these phenomena. Extending this method to 3 sites is prohibitive as this will entail an expansion in $4^3 = 64$ three-site eigenstates. This calculation is impossible as the complexity of the two-site problem is already daunting. What does seem promising, however, is a possible field theory description of the local dynamics that seem to be essential to an accurate description of strong correlation physics. Work along these lines as well as extending the present method to the doped case is underway.

ACKNOWLEDGMENTS

We could not have completed this work without the generous help of F. Mancini and H. Matsumoto who sent us previous more detailed versions of their work. A special thanks goes also to H. Matsumoto who also sent us his computer program after we had struggled several months to reproduce the results of Ref. ([10]). As a result, we were able to determine the source of the difference between our results [11]. We also thank the NSF grant No. DMR98-96134 for partially funding this work.

-
- [1] S. White, D. J. Scalapino, R. L. Sugar, E. Y. Loy, J. E. Gubernatis, and R. T. Scalettar, Phys. Rev. B **40**, 506 (1989);
 - [2] N. F. Mott, Metal-Insulator Transitions (Taylor & Francis, 1974).
 - [3] W. F. Brinkman and T. M. Rice, Phys. rev. B **2**, 4302 (1970).
 - [4] M. Vekic and S. R. White, Phys. Rev. B **47**, 1160 (1993); F. Mancini, Euro. Phys. Lett. **50**, 229-35 (2000).
 - [5] C. Castellani, C. D. Castro, D. Feinberg, and J. Ranninger, Phys. Rev. Lett. **43**, 1957 (1979).
 - [6] G. Kotliar and A. E. Ruckenstein, Phys. Rev. Lett. **57** 1362 (1986); ; R. Fresard and P. Wölfle, Int. J. Mod. Phys. B **6**, 685 (1992);
 - [7] For a review see A. Georges, G. Kotliar, W. Krauth, and M. J. Rozenberg, Rev. Mod. Phys. **68**, 13 (1996).
 - [8] P. W. Anderson, *The Theory of Superconductivity in the High- T_c Cuprates* (Princeton series in Physics, Princeton University Press, 1997), pp. 291-294.
 - [9] E. H. Lieb and F. Y. Wu, Phys. Rev. Lett. **53**, 194 (1984).
 - [10] H. Matsumoto and F. Mancini, Phys. Rev. B **55**, 2095 (1997).
 - [11] Our implementation of the two-site approximation to the dynamical corrections **does** in fact differ from that of Matsumoto and Mancini in the previous reference. In their computer program, an off-diagonal matrix element in the resolvents for FF and DB enters with the **wrong** sign. This simple error took about 4 months to find and

leads to substantial differences in the dynamical corrections. As a result, the present study represents the first correct implementation of the two-site approximation to the dynamics in the Hubbard model.

- [12] S. Moukouri and M. Jarrell, cond-mat/0011247.
- [13] N. Kawakami, T. Usuki, and A. Okiji, Phys. Lett. A **137**, 287 (1989).
- [14] A. Georges and W. Krauch, Phys. Rev. B **48**, 7167 (1993).
- [15] D. Duffy and A. Moreo, Phys. Rev. B **55**, 12918 (1997).
- [16] D. Vollhardt, Phys. Rev. Lett. **78**, 1307 (1997); See also, N. Chandra, M. Kollar, and D. Vollhardt, Phys. Rev. B **59**, 10541 (1999).
- [17] D. F. Brewer, J. G. Daunt, and A. K. Sreedhar, Phys. Rev. **115**, 836 (1959); D. S. Greywall, Phys. Rev. B **27**, 2747 (1983).
- [18] H. G. Schlager, A. Schröder, M. Welsch, and H. v. Löhneysen, J. Low Temp. Phys. **90**, 181 (1993).
- [19] T. Brugger, T. Schreiner, G. Roth, and G. Czjzek, Phys. Rev. Lett. **71**, 2481 (1993).
- [20] N. E. Phillips, R. A. Fisher, J. Floquet, A. L. Giorgi, J. A. Olsen, and G. R. Stewart, J. Magn. Magn. Mater. **63&64**, 332 (1987).
- [21] S. Avella, et al. Int. J. Mod. Phys. **12**, 81 (1998).
- [22] L. M. Roth, Phys. Rev. **184**, 451 (1969).
- [23] T. Stanescu, I. Martin, and P. Phillips, Phys. Rev. B **62**, 4300-4308 (2000).
- [24] Y. Kuramoto, Z. Phys. B **53**, 37 (1983).
- [25] G. Kotliar, E. Lange, and M. J. Rozenberg, cond-mat/0003016.
- [26] H. Shiba and P. A. Pincus, Phys. Rev. B **5**, 1966 (1972).
- [27] T. Paiva, R. T. Scalettar, C. Huscroft, and A. K. McMahhan, Phys. Rev. B Phys. Rev. B **63**, 125116 (2001).